Original Article

MOLECULAR METABOLISM

Ceramides are necessary and sufficient for diet-induced impairment of thermogenic adipocytes

Bhagirath Chaurasia [1,2,*], Li Ying [2], Chad Lamar Talbot [2], John Alan Maschek [3], James Cox [3], Edward H. Schuchman [4], Yoshio Hirabayashi [5], William L. Holland [2], Scott A. Summers [2]

ABSTRACT

Objective: Aging and weight gain lead to a decline in brown and beige adipocyte functionality that exacerbates obesity and insulin resistance. We sought to determine whether sphingolipids, such as ceramides, a class of lipid metabolites that accumulate in aging and overnutrition, are sufficient or necessary for the metabolic impairment of these thermogenic adipocytes.

Methods: We generated new mouse models allowing for the conditional ablation of genes required for ceramide synthesis (i.e., serine palmitoyltransferase subunit 2, *Sptlc2*) or degradation (i.e., acid ceramidase 1, *Asah1*) from mature, thermogenic adipocytes (i.e., from cells expressing uncoupling protein-1). Mice underwent a comprehensive suite of phenotyping protocols to assess energy expenditure and glucose and lipid homeostasis. Complementary studies were conducted in primary brown adipocytes to dissect the mechanisms controlling ceramide synthesis or action.

Results: Depletion of *Sptlc2* increased energy expenditure, improved glucose homeostasis, and prevented diet-induced obesity. Conversely, depletion of *Asah1* led to ceramide accumulation, diminution of energy expenditure, and exacerbation of insulin resistance and obesity. Mechanistically, ceramides slowed lipolysis, inhibited glucose uptake, and decreased mitochondrial respiration. Moreover, β-adrenergic receptor agonists, which activate thermogenesis in brown adipocytes, decreased transcription of enzymes required for ceramide synthesis.

Conclusions: These studies support our hypothesis that ceramides are necessary and sufficient for the impairment in thermogenic adipocyte function that accompanies obesity. Moreover, they suggest that implementation of therapeutic strategies to block ceramide synthesis in thermogenic adipocytes may serve as a means of improving adipose health and combating obesity and cardiometabolic disease.

Keywords Ceramides; Sphingolipids; brown adipose tissue; Obesity; Insulin resistance; Diabetes

1. INTRODUCTION

Brown adipose tissue (BAT) is a highly active metabolic organ that has a profound impact on body habitus and risk for diabetes and cardiovascular disease. BAT contains an extensive blood supply that delivers nutrients to brown adipocytes enriched in mitochondria and small, labile lipid droplets [1–4]. These unique adipocytes dissipate energy by generating heat through uncoupled respiration, a process mediated by uncoupling protein-1 (UCP1) [5]. Thermogenic adipocytes that conditionally express UCP1 (i.e., beige adipocytes) can also be found in white adipose tissue depots [6,7]. The quantity and activity of these thermogenic, UCP1^{+} adipocytes inversely correlate with age and adiposity in humans and rodents [8–12], leading investigators to speculate that their disruption may contribute to the obesity epidemic. Motivated by these observations, researchers have sought to identify strategies to activate thermogenic adipocytes to treat obesity and its metabolic comorbidities.

Obesity occurs when fuel consumption exceeds fuel use, with the excess nutritional energy stored primarily in fatty acids. Newly synthesized or absorbed free fatty acids are immediately coupled to coenzyme A and then incorporated into macromolecules, such as glycerolipids and sphingolipids. The glycerolipids, which include the triglycerides that are the major energy reservoir in the body and the glycerophospholipids that form the bulk of cell membranes (e.g., phosphatidylcholine, phosphatidylethanolamine, etc.), are produced through a biosynthetic pathway involving the sequential addition of acyl-CoAs to a glycerol backbone. The less abundant sphingolipids are generated by the addition of acyl-CoAs to an alternative, sphingoid scaffold derived from amino acids (e.g., serine). Herein, we demonstrate that intermediates in the sphingolipid biosynthesis pathway, particularly the ceramides, are cues of nutritional excess that regulate thermogenic adipocytes to influence energy utilization and expenditure.

The sphingolipid biosynthesis pathway starts with the condensation of an amino acid and fatty acid, most typically serine and palmitate [13].

[1]Division of Endocrinology, Department of Internal Medicine, Carver College of Medicine, Fraternal Order of Eagles Diabetes Research Center, University of Iowa, Iowa City, IA, 52242, USA [2]Department of Nutrition and Integrative Physiology and the Diabetes and Metabolism Research Center, University of Utah, Salt Lake City, UT, USA [3]Department of Biochemistry, University of Utah, Salt Lake City, UT, USA [4]Department of Genetics and Genomic Sciences, Mount Sinai School of Medicine, New York, USA [5]RIKEN Brain Science Institute, Wako-Shi, Saitama Japan

*Corresponding author. Division of Endocrinology, Department of Internal Medicine, Carver College of Medicine, Fraternal Order of Eagles Diabetes Research Center, University of Iowa, Iowa City, IA, 52242, USA. E-mail: bhagirath-chaurasia@uiowa.edu (B. Chaurasia).

Received October 12, 2020 • Revision received November 25, 2020 • Accepted December 14, 2020 • Available online 19 December 2020

https://doi.org/10.1016/j.molmet.2020.101145

This reaction is catalyzed by the enzyme serine palmitoyltransferase, which has three essential subunits (SPTLC1, 2, and 3) and several other regulatory proteins that control substrate specificity. In a subsequent step of this enzymatic cascade, ceramide synthases (CERS1-6) add variable fatty acids to this scaffold, producing a diverse family of dihydroceramides. Dihydroceramide desaturases then insert an essential double bond to produce the ceramides, which are the first sphingolipid to accrue in substantial quantities and fundamental building blocks of complex sphingolipids, such as sphingomyelins, ceramide-1-phosphate, and gangliosides. Ceramides are deacylated by a family of ceramidases, including the acid ceramidase, that we manipulated herein.

Numerous studies have shown that ceramides increase in people with obesity or metabolic disease [14–19]. Moreover, inhibiting serine palmitoyltransferase or dihydroceramide desaturase-1 in rodents lowers ceramides and ameliorates most of the comorbidities of obesity, including insulin resistance, diabetes, atherosclerosis, and non-alcoholic fatty liver disease [20–27]. We have previously speculated that some of these beneficial attributes of ceramide depletion result from autonomous effects within the adipocyte. For example, we demonstrated that depleting *Sptlc2* from adipocytes (i.e., using an adiponectin-Cre transgenic mouse from Philipp Scherer at UT Southwestern) increases glucose uptake and energy expenditure) [14]. In opposition to our study, two other groups found that depleting *Sptlc2* or *Sptlc1* from adipose tissue, using a different adiponectin-Cre transgenic mouse line (generated by Evan Rosen and sold by Jackson Laboratories), induced lipodystrophy [28,29]. We speculated that the discrepancy might be due to differences in the adiponectin promoter fragment used to induce Cre-recombinase and perhaps the timing of gene depletion in relation to adipocyte development. We and others have shown that SPT inhibitors inhibit adipocyte differentiation of preadipocytes studied *in vitro* [14]. Nonetheless, the role of ceramides in terminally differentiated adipocytes *in vivo* has remained unclear and controversial.

To bypass sphingolipid actions on adipocyte differentiation, we modulated *Sptlc2* using a transgenic mouse expressing *Ucp1*-driven Cre, which allowed us to determine whether sphingolipids, such as ceramides, were necessary for diet-induced impairment of terminally differentiated thermogenic adipocytes. We also tested whether increasing ceramide levels in thermogenic adipocytes (i.e., by depleting acid ceramidase from *Ucp1*-expressing cells) in mice was sufficient to induce metabolic dysfunction. Lastly, we evaluated the effects of overexpressing a gene that produces ceramides (i.e., ceramide synthase-6, CERS6) in differentiated brown adipocytes. The data obtained using these models clearly reveal that sphingolipids, such as ceramides, are both sufficient and necessary for diet-induced impairment of tissue function and disruption of organismal glucose and lipid metabolism. These findings support the possibility that inhibiting sphingolipid biosynthesis in thermogenic adipocytes could serve as an attractive therapeutic strategy to improve metabolic health.

2. MATERIAL AND METHODS

2.1. Animal care

Animal procedures were conducted in compliance with protocols approved by the Institutional Animal Care and Use Committee (IACUC) at the University of Utah. Mice were housed in groups of 3–5 at 22–24 °C or at thermoneutrality (30 °C) using a 12-hour light/12-hour dark cycle. Animals had *ad libitum* access to water at all times. Animals were fed a normal chow diet (NCD) or high-fat diet (HFD) (D12492; Research Diets Inc., New Brunswick, NJ) from the age of 4 weeks as indicated.

2.2. Generation of $Sptlc2^{\delta Ucp1}$ mice

To delete *Sptlc2* from brown adipocytes, $Sptlc2^{loxP/loxP}$ mice [14] were crossed with mice expressing Cre-recombinase under the control of the uncoupling protein1 gene (*Ucp1*) promoter [30]. Breeding $Sptlc2^{loxP/loxP}Ucp1\text{-Cre}^{-/-}$ mice with $Sptlc2^{loxP/loxP}Ucp1\text{-Cre}^{+/-}$ produced mice with brown adipocyte-specific *Sptlc2* deletion and littermate controls (denoted as $Sptlc2^{\delta Ucp1}$ mice and Control, respectively).

2.3. Generation of $Asah1^{\delta Ucp1}$ mice

To delete *Asah1* from brown adipocytes, $Asah1^{loxP/loxP}$ mice [31] were backcrossed onto a C57Bl6/J background using speed congenic services from Jackson Labs and then further crossed with mice expressing Cre-recombinase under the control of the uncoupling protein-1 gene (*Ucp1*) promoter [30]. Breeding $Asah1^{loxP/loxP}Ucp1\text{-Cre}^{-/-}$ mice with $Asah1^{loxP/loxP}Ucp1\text{-Cre}^{+/-}$ produced mice with brown adipocyte specific *Asah1* deletion and littermate controls (denoted as $Asah1^{\delta Ucp1}$ mice and Control, respectively).

2.4. Glucose and insulin tolerance tests

Glucose tolerance tests were performed in 16-week-old mice after an overnight fast. Glucose was injected (intraperitoneal injection of a 20% solution, 10 mL/kg body weight), and blood glucose concentrations were measured after 0, 15, 30, 60, and 120 min with a glucometer. Insulin tolerance tests were performed in 14-week-old mice fed *ad libitum*. After determination of basal blood glucose concentrations, each mouse received an intraperitoneal injection of insulin (0.75 IU per kg body weight; Actrapid; Novo Nordisk) and blood glucose concentrations were measured after 15, 30, 45, and 60 min.

2.5. Analysis of body composition

Lean and fat mass were determined via NMR™ (Bruker, Germany) in live, 12- to 18-week-old mice.

2.6. Indirect calorimetry

Metabolic measurements were obtained using the CLAMS (Columbus Instruments) open-circuit indirect calorimetry system. Food and water were provided *ad libitum* in the appropriate devices and measured by the built-in automated instruments. Animals were allowed to acclimatize to the cages for at least 12 h before data acquisition for an additional 24 h.

2.7. BAT surface temperature

BAT surface temperature was measured using an infrared camera (C2; FLIR; West Malling, Kent, UK) and FLIR-Tools-Software (FLIR; West Malling, Kent, UK).

2.8. Analytical procedure

Blood glucose levels were determined from whole venous blood using an automatic glucose monitor (Bayer Contour, Bayer, Germany). Blood glucose levels were determined from whole venous blood using an automatic glucose monitor (Bayer Contour, Bayer, Germany). Insulin levels in serum were measured by Alpco insulin enzyme-linked immunosorbent assay (ELISA) assay using mouse standards according to the manufacturer's guidelines (Alpco).

2.9. Stromal vascular culture (SV) and primary brown adipocyte differentiation

Interscapular brown fat pads from 2 or 3 mice (4–6 fat pads total, 5- to 6-week-old male mice) were dissected, washed, minced, and then pooled and digested for 30–45 min at 37°C in phosphate-buffered saline (PBS) containing 10 mM of $CaCl_2$, 3 mg/mL collagenase (Sigma). Digested tissues were filtered through a 100-μm-cell strainer to remove undigested tissues. The flow-through was then centrifuged at 1,200 rpm for 5 min to pellet the SV cells. Following further centrifugation at the above-mentioned speed, the SV cells were re-suspended in complete SV culture medium (Dulbecco's modified Eagle's medium (DMEM)/F12 [1:1; Invitrogen] plus Glutamax, pen/strep, and 10% fetal bovine serum (FBS)) and then further filtered through a 40-μm cell strainer to remove clumps and large adipocytes. The SV's were further treated with red cell lysis buffer (Sigma) to remove the red blood cells. Following further centrifugation as mentioned above, SV cells were then re-suspended in SV culture medium and plated onto a 6-cm tissue culture dish. For brown adipocyte differentiation assays, SV cells were plated and grown to confluence in SV culture medium. At confluence (day 0), cells were exposed to a differentiation cocktail containing 5 μM of dexamethasone (Sigma), 0.05 μM of insulin (Gibco), 0.5 mM of isobutylmethylxanthine (Sigma), 1 nM of T3, 125 nM of indomethacin (Sigma) and 1 μM rosiglitazone (Sigma) in the culture medium. Forty-eight hours after induction, cells were maintained in SV culture medium containing 0.05 μM of insulin (Gibco) and 1 nM of T3 (Sigma). At day 8 of the differentiation, 10 μM of myriocin (Sigma) was also supplemented for the next 6 h. For isoproterenol treatments, cells were treated with 1 μM or 5 μM of isoproterenol for indicated times. For forskolin treatments, cells were treated with 10 μM or 20 μM of forskolin (Sigma) for the indicated times. For seahorse experiments, the cells were trypsinized on day 8 and plated into the 24-well seahorse plates as described above. After 24 h, the media containing C_2-ceramides (25 and 50 μM) was added. After 6 h, the oxygen consumption rates were determined.

2.10. Adenovirus infection in primary brown adipocytes

Brown adipocytes were differentiated in a 6-well plate, and recombinant adenovirus expressing either green fluorescent protein (GFP) or mouse *CerS6* (6×10*8 PFUs) were added to each well. All analyses were performed 48 h post adenovirus infection. Adenoviruses were procured from Viraquest, Inc., USA.

2.11. Adipose tissue respiration, mitochondrial complex activity, and β-oxidation

Tissue respiration was performed using an O2K high-resolution respirometer (Oroboros, Austria). Freshly isolated tissues were rapidly weighed (BAT 2–5 mg), minced, and homogenized using a PBI-shredder PBI set (Oroboros, Austria). Homogenized tissue was further re-suspended in 2 mL of MiR05 medium (0.5 mM of EGTA, 3 mM of MgCl2, 60 mM of K-lactobionate, 20 mM of Taurine, 10 mM of KH_2PO_4, 20 mM of HEPES, 110 mM of Sucrose, and 1 g/L of BSA (essentially fatty acid free)). Respiratory oxygen flux was measured in real time and expressed as picomoles of O_2 per second per mg of tissue. 5 mM of pyruvate (Sigma), 2 mM of malate (Sigma), and 1 mM of ADP (Sigma) were added to stimulate complex I respiration. 1 μM of rotenone (Sigma) and 5 mM of succinate (Sigma) were added to test complex II respiration. 2 mM of ascorbate and 0.5 mM of N, N, N, N-tetramethyl-p-phenylenediamine (TMPD) (Sigma) were used to test complex IV respiration. To measure uncoupled respiration, succinate (Sigma) was used as the substrate, and 1 μM of oligomycin (Sigma) was added to determine the coupled respiration. Uncoupled respiration was calculated using the respiration rate after oligomycin deducted by respiration rate after antimycin A (1 μM) (Sigma) inhibition. To measure mitochondrial β-oxidation, palmitoyl-carnitine (5 μM) (Sigma) was added to the chamber.

2.12. Cellular oxygen consumption

Cellular oxygen consumption rates were measured using the Seahorse XF24 analyzer. Differentiated adipocytes were seeded into coated Seahorse XF24 cell culture plates at a density of 40,000 cells/well and incubated overnight. Cells were then washed and changed to assay running media (unbuffered RPMI 1640 buffer with 11 mM of glucose) before being incubated in a non-CO_2 incubator at 37 °C for 60 min. The basal oxygen consumption rate was measured using the fixed delta technique over 3 measurement periods, each comprised of a 4-minute mix, 2-minute wait, and 2-minute measurement. Test compounds were obtained from Seahorse Bioscience and injected during the assay, including the following: 1 μg/μL of oligomycin, 0.3 μM of FCCP (carbonyl cyanide 4-(trifluoromethoxy) phenylhydrazone), 1 μM of rotenone, and 10 μM of antimycin A. At the end of the assay, cells were washed twice with PBS and lysed for protein quantification. Oxygen consumption values were then normalized to protein concentration. The basal and percentage of oxygen consumption rate as well as area under the curve value were obtained using XF24 Analyzer software.

2.13. Lipidomics

Lipid extracts were separated as we described previously [20] on an Acquity UPLC CSH C18 1.7 μm 2.1 × 50 mm column maintained at 60 °C connected to an Agilent HiP 1290 Sampler, Agilent 1290 Infinity pump, equipped with an Agilent 1290 Flex Cube, and Agilent 6490 triple quadrupole (QqQ) mass spectrometer. Sphingolipids were detected using dynamic multiple reaction monitoring (dMRM) in the positive ion mode. Source gas temperature was set to 210 °C, with a gas (N_2) flow of 11 L/min and a nebulizer pressure of 30 psi. Sheath gas temperature was 400 °C, sheath gas (N_2) flow of 12 L/min, capillary voltage was 4000 V, nozzle voltage 500 V, high pressure RF 190 V, and low-pressure RF was 120 V. Injection volume was 2 μL, and the samples were analyzed in a randomized order with the pooled QC sample injection 8 times throughout the sample queue. Mobile phase A consisted of ACN: H2O (60:40 v/v) in 10 mM of ammonium formate and 0.1% formic acid, and mobile phase B consists of IPA: ACN:H_2O (90:9:1 v/v) in 10 mM of ammonium formate and 0.1% formic acid. The chromatography gradient started at 15% mobile phase B, increased to 30% B over 1 min, increased to 60% B from 1 to 2 min, increased to 80% B from 2 to 10 min, and increased to 99% B from 10 to 10.2 min, where it was held until 14 min. Post-time was 5 min, and the flow rate was 0.35 mL/min throughout. Collision energies and cell accelerator voltages were optimized using sphingolipid standards with dMRM transitions as $[M+H]^+ \rightarrow [m/z = 284.3]$ for dihydroceramides, $[M+H]^+ \rightarrow [m/z = 287.3]$ for isotope-labeled dihydroceramides, $[M-H_2O + H]^+ \rightarrow [m/z = 264.2]$ for ceramides, $[M-H_2O + H]^+ \rightarrow [m/z = 267.2]$ for isotope-labeled ceramides and $[M+H]^+ \rightarrow [M-H_2O + H]+$ for all targets. Sphingolipids without available standards were identified based on high-resolution liquid chromatography mass spectrometry (HR-LC/MS), quasi-molecular ion and characteristic product ions. Their retention times were either taken from HR-LC/MS data or inferred from the available sphingolipid standards. Results from LC-MS experiments were collected using an Agilent Mass Hunter Workstation and analyzed using the software package Agilent Mass Hunter Quant B.07.00. Sphingolipids were quantitated based on peak area ratios to the standards added to the extracts.

2.14. Quantitative reverse transcription polymerase chain reaction (RT-PCR)

Total RNA was extracted from respective tissues and cells using the RNeasy Mini Isolation Kits with DNA digestion (QIAGEN) according to the manufacturer's instructions. Isolated total RNA was reverse-transcribed into cDNA using commercially available kits (Biorad). All subsequent qRT-PCR reactions were performed on a QuantStudio 12K Flex Real-Time PCR system (Thermo Fisher Scientific) using the Qiagen QuantiFast SYBR Green PCR kit. For normalization, threshold cycles (C_t-values) of all replicate analyses were normalized to *Hprt* or *Actb* within each sample to obtain sample-specific ΔC_t values (= C_t gene of interest - C_t *Hprt*, Actin). To compare the effect of various treatments with untreated controls, $2^{-\Delta\Delta Ct}$ values were calculated to obtain fold expression levels, where $\Delta\Delta C_t = (\Delta C_t$ treatment - ΔC_t control).

2.15. Mouse qRT-PCR primer sequences and Taqman probes

The following primer sequences, which were validated previously, were used in this study [14,20]:

Actb: Fwd: 5′-GAT GTA TGA AGG CTT TGG TC-3′, Rev: 5′-TGT GCA CTT TTA TTG GTC TC-3′, ***Asah1***: Fwd: 5′ TAA CCG CAG AAC ACC GGC C-3′, Rev: 5′- TTG ACC TTT GGT AAC ATC CAT C-3′,***Hprt***: Fwd: 5′-AGG GAT TTG AAT CAC GTT TG-3′, Rev: 5′-TTT ACT GGC AAC ATC AAC AG-3′, ***Sptlc1:*** Fwd: 5′-AGG GTT CTA TGG CAC ATT TGA TG-3′, Rev: 5′-TGG CTT CTT CGG TCT TCA TAA AC-3′, ***Sptlc2:*** Fwd: 5′- CAA AGA GCT TCG GTG CTT CAG-3′, Rev: 5′-GAA TGT GTG CGC AGG TAG TCT ATC-3′, ***Ucp1:*** Fwd: 5′-ACT GCC ACA CCT CCA GTC ATT-3′, Rev: 5′-CTT TGC CTC ACT CAG GAT TGG-3′, ***Dio2:*** Fwd: 5′-CAG TGT GGT GCA CGT CTC CAA TC-3′, Rev: 5′-TGA ACC AAA GTT GAC CAC CAG-3′, ***Ppargc1a:*** Fwd: 5′-CCC TGC CAT TGT TAA GAC C-3′, Rev: 5′-TGC TGC TGT TCC TGT TTT C-3′, ***Cidea:*** Fwd: 5′-GCC GTG TTA AGG AAT CTG CTG-3′, Rev: 5′-TGC TCT TCT GTA TCG CCC AGT-3′, ***Prdm16:*** Fwd: 5′-CAG CAC GGT GAA GCC ATT C-3′, Rev: 5′-GCG TGC ATC CGC TTG TG-3′, ***Pgc1a:*** Fwd: 5′-CCC TGC CAT TGT TAA GAC C-3′, Rev: 5′-TGC TGC TGT TCC TGT TTT C-3′, ***Pgc1b:*** Fwd: 5′-TCC TGT AAA AGC CCG GAG TAT-3′, Rev: 5′-GCT CTG GTA GGG GCA GTG A-3′, ***Cox7a:*** Fwd: 5′-CAG CGT CAT GGT CAG TCT GT-3′, Rev: 5′-AGA AAA CCG TGT GGC AGA GA-3′, ***Cox8b:*** Fwd: 5′-GAA CCA TGA AGC CAA CGA CT-3′, Rev: 5′-GCG AAG TTC ACA GTG GTT CC-3′, ***Cpt1a:*** Fwd: 5′-ACG TTG GAC GAT CGG AAC A-3′, Rev: 5′-GGT GGC CAT GAC ATA CTC CC-3′, ***Fasn:*** Fwd: 5′-TGC TCC AGG GAT AAC AGC-3′, Rev: 5′-CCA AAT CCA ACA TGG GAC A-3′, ***Lipe:*** Fwd: 5′-GGA GCA CTA CAA ACG CAA CGA-3′, Rev: 5′-TCG GCC ACC GGT AAA GAG-3′, ***Srebp1c:*** Fwd: 5′-ATC GGC GCG GAA GCT GTC GGG GTA GCG TC-3′, Rev: 5′-ACT GTC TTG GTT GTT GAT GAG CTG GAG CAT-3′, ***Atgl:*** Fwd: 5′-AAC ACC AGC ATC CFG TTC AA-3′, Rev: 5′-GGT TCA GTA GGC CAT TCC TC-3′, and other primer sequences can be provided on request.

2.16. Histology and immunochemistry

For histology, tissues were fixed in 10% formalin for 48 h, embedded in paraffin, sectioned at 5 μm, and stained with hematoxylin and eosin or immunostained with antibodies directed against UCP1 (Abcam: ab10983) as previously described [20]. Quantification of cell size was performed with ImageJ software (NIH).

2.17. Transmission electron microscopy

Freshly dissected BATs were minced into small pieces and fixed in primary fixation media (1% glutaraldehyde, 2.5% paraformaldehyde, 100 mM of cacodylate buffer, pH 7.4, 6 mM of $CaCl_2$ and 4.8% sucrose) at 4 °C overnight. The next day, following washes with cacodylate buffer, 100 mM, pH 7.4, the tissues were fixed in secondary fixation media (cacodylate buffer and 2% osmium tetroxide) at room temperature for 1 h. The tissues were subsequently washed and then pre-stained with saturated uranyl acetate for 1 h at room temperature, followed by dehydration with graded and absolute acetone. The tissues were then infiltrated with Epon epoxy resin and polymerized for 48 h at 60 °C. Tissue sections of 70 nm thickness were cut using Leica UC 6 ultratome and mounted on 200 mesh copper grids. The grids with the sections were stained for 20 min with saturated uranyl acetate and 10 min with lead citrate. Sections were examined at an accelerating voltage of 120 kV in a JEOL-1400 plus (JEOL, Japan) transmission electron microscope equipped with a CCD Gatan camera.

2.18. Assessment of β-adrenergic signaling

Differentiated adipocytes were treated with 50 μM of C_2-ceramide or C_6-dihydroceramide for 4 h. The cells were then treated with 10 μM of isoproterenol for 30 min, and cells were analyzed for β-adrenergic signaling intermediates pHSL, HSL, and pPKA substrates by western blot. To inhibit PP2A activity, following 4 h of treatment with 50 μM of C_2-ceramide, the cells were treated with 25 nM of microcystin-LR for 1 h. The cells were then treated with isoproterenol as mentioned above. HSL phosphorylation was assessed via immunoblotting. The following antibodies were used: phospho-HSL (Ser563), Cell Signaling, catalog number: 4139, HSL, Cell Signaling, catalog number: 4107, phospho-PKA: phospho-PKA Substrate (RRXS*/T*) (100G7E), Cell Signaling, catalog number: 9624, β-actin: beta-actin (8H10D10), Cell Signaling, catalog number: 3700S.

2.19. Insulin signaling

Differentiated primary brown adipocytes in 12-well plates were fasted for 2 h in a DMEM media lacking FBS. Thereafter, cells were treated with 50 μM of C_2-ceramide for 4 h and then treated with 10 nM of insulin for 30 min. Akt phosphorylation was determined via immunoblotting. The following antibodies were used: pAkt S473, Cell Signaling, catalog number: 4051S, Akt, Cell Signaling, catalog number: 9272, β-Actin: Beta-Actin (8H10D10), Cell Signaling, catalog number: 3700S.

2.20. FFA uptake assay

Primary brown adipocytes were differentiated in a 96-well plate. Post-differentiation, cells were serum starved for 1 h. Thirty minutes prior to beginning the assay, cells were treated with vehicle or 1 μM of isoproterenol (Thermo Fisher Scientific #41400045). Fatty acid uptake was then measured using the Molecular Devices QBT Fatty Acid Uptake Assay Kit according to manufacturer instructions.

2.21. Measurement of sphingolipid flux using stable isotopes

Fully differentiated primary brown adipocytes in a 12-well plate were switched to minimum essential media (MEM) lacking serine for 2 h. The cells were then switched to MEM containing 0.4 mM of L-serine-$^{13}C_3$,^{15}N and variable concentrations of isoproterenol for the 3, 6, 12, and 24 h. The reaction was then washed with PBS, trypsinized, and stored at −80 °C. Lipids were thereafter extracted and analyzed by mass spectrometry at the University of Utah Metabolomics Core.

2.22. Western blot analysis

Proteins were extracted from tissues or cultured cells by homogenizing or scraping in radioimmunoprecipitation assay (RIPA) buffer (0.5% NP-40, 0.1% sodium deoxycholate, 150 mM of NaCl, 50 mM of Tris—HCl, pH 7.5) containing protease inhibitors (Complete Mini, Roche). The homogenate was cleared by centrifugation at 4 °C for 30 min at 15,000 *g* and the supernatant containing the protein fraction recovered. Protein concentration in the supernatant was determined using

the BCA Protein Assay Kit (Pierce). Twenty micrograms of protein was resolved using precast Bolt or NuPAGE (4–12% Bis-Tris gels, Invitrogen) and transferred to nitrocellulose membranes (GE Healthcare). Membranes were blocked with 5% BSA in Tris-buffered saline containing 0.2% Tween-20 (tris-buffered saline with Tween, TBS-T) and incubated with primary antibodies at 4 °C overnight.

2.23. Statistics

Data are generally plotted as the mean ± SEM. Student *t*-test or one-way or two-way analysis of variance (ANOVA) were carried out using Prism (GraphPad Prism), and statistical significance was considered meaningful at $p < 0.05$.

3. RESULTS

3.1. Reciprocal regulation of ceramides by obesogenic diets and β-adrenergic stimuli in brown adipocytes

Using mass spectrometry, we quantified levels of 38 sphingolipids in BAT isolated from C57Bl6/J mice fed an NCD or an obesogenic HFD for 12 weeks. Consumption of the obesogenic diet increased levels of the C_{16}-ceramides (Figure 1A) that have been found to be key regulators of metabolic homeostasis [32–36]. Other sphingolipids, sphingomyelins, dihydroceramides, sphingosine, and sphinganine were unaffected (Suppl. Figure 1A–D). More polar sphingolipids, such as sphingosine-1-phosphate, ceramide-1-phosphate, and gangliosides, were not measured by this method.

We next evaluated whether the ceramide pool might be modulated acutely by factors known to influence activity of thermogenic brown and beige adipocytes [37]. To quantify rapid changes in rates of ceramide biosynthesis, we used a flux assay that monitors the incorporation of $C_{13}N_{15}$-labeled serine into the sphingolipid backbone [20]. Treating primary brown adipocytes with isoproterenol, an agonist of the β-adrenergic receptors, which increase thermogenesis, dramatically slowed biosynthesis rates of many different ceramide species (Figure 1B and Suppl. Figure 1E–I). This effect was due to isoproterenol's ability to reduce expression of serine palmitoyltransferase-2 (*Sptlc2*) and ceramide synthase-6 (*CerS6*), but not other enzymes in the pathway (i.e., dihydroceramide desaturase-1, *Degs1*) (Figure 1C). Forskolin, which activates an essential intermediate in β-adrenergic signaling (i.e., adenylate cyclase), recapitulated the effects on *Sptlc2* and *CerS6* (Figure 1D).

3.2. Inhibition of ceramide biosynthesis in UCP1$^+$-cells increases energy expenditure in mice housed at ambient temperature

We crossed mice containing a floxed *Sptlc2* (*Sptlc2*$^{fl/fl}$) allele [14] with ones expressing Cre-recombinase under the control of the UCP1 promoter [30]. The resultant *Sptlc2*$^{\delta Ucp1}$ mice had small but significantly reduced levels of *Sptlc2* transcripts, but not *Sptlc1*, in BAT. Under these conditions, *Sptlc2* levels in subcutaneous (sWAT) depots were not significantly altered, although they trended in a downward direction (Figure 1E). Despite these small changes in *Sptlc2* transcripts, ceramide content was reduced by 50–60% (Figure 1F) in both BAT and sWAT depots. Remarkably, serum levels were also diminished. The changes in sWAT were expected due to the presence of beige adipocytes that conditionally express UCP-1. The reduced serum levels of ceramide suggest UCP1$^+$ thermogenic adipocytes contribute significantly to the pool of circulating ceramides, an idea that is consistent with prior observation [14]. Ceramide levels were unchanged in non-UCP-1-containing tissues such as epididymal WAT (eWAT), liver, or skeletal muscle (Figure 1E, and 1F). Other sphingolipids, including the more abundant sphingomyelins were not substantially diminished by *Sptlc2* depletion (Suppl. Figure 2A–D). These data are consistent with our prior findings that the less-abundant, intermediary sphingolipids, such as ceramides, are more dynamically regulated by changes in flux and fatty acid availability than more abundant complex sphingolipids, such as sphingomyelins [38].

Four-week-old *Sptlc2*$^{\delta Ucp1}$ and *Sptlc2*$^{fl/fl}$ (control) mice were fed control (NCD) or obesogenic high-fat (HFD) diets for 12 weeks while being housed under ambient temperature (22 °C). On an NCD, the effects of *Sptlc2* depletion were marginal; the *Sptlc2*$^{\delta Ucp1}$ animals contained slightly smaller BAT depots (Figure 1I) than *Sptlc2*$^{fl/fl}$ littermates, but otherwise had comparable body weights (Figure 1G), lean and fat mass (Figure 1H), and eWAT/sWAT/liver weights (Figure 1I). They had reduced locomotor activity, but otherwise displayed no alterations in oxygen consumption (VO_2), carbon dioxide production (VCO_2), energy expenditure, respiratory exchange ratio (RER), and food intake (Suppl. Figure 2E–K). Unlike the animals maintained on the NCD, the *Sptlc2*$^{\delta Ucp1}$ mice fed the HFD displayed a significant phenotype. They were partially protected from obesity (Figure 1G) showing less total fat mass (Figure 1H) and reduced BAT, sWAT, and liver weights (Figure 1I). The *Sptlc2*$^{\delta Ucp1}$ animals receiving the HFD also exhibited increased VO_2, VCO_2, energy expenditure and food intake compared to the *Sptlc2*$^{fl/fl}$ controls (Figure J–M). No changes were observed for lean mass (Figure 1H), RER, or locomotor activity (Suppl. Fig. 2M–O). Depletion of *Sptlc2* from UCP1-containing adipocytes partially resolved the metabolic impairments caused by obesity. The *Sptlc2*$^{\delta Ucp1}$ knockout animals maintained on the obesogenic diet displayed improved glucose tolerance (Figure 2A), enhanced glucose disposal during an insulin-tolerance test (Figure 2B), and diminished insulin levels (Figure 2C), as compared to the *Sptlc2*$^{fl/fl}$ controls.

Histological assessment revealed that ablation of *Sptlc2* from UCP-1$^+$-cells produced a broad spectrum of morphological effects. The BAT and sWAT depots were smaller (Figure 2D–E) and liver fat was reduced (Figure 2D) in the *Sptlc2*$^{\delta Ucp1}$ animals compared to *Sptlc2*$^{fl/fl}$ controls. Moreover, *Sptlc2*$^{\delta Ucp1}$ mice exhibited reductions in various liver transcripts associated with steatosis (e.g., *F4/80*, *Ccl2*, *Cd36, Cidea*, *and Pparg)* (Figure 2F). Collectively, these data indicate that sphingolipids in UCP1$^+$-cells, most likely ceramides, were required for diet impairment of UCP1$^+$-cell function and the development of obesity.

Housing mice at 22 °C results in chronic activation of BAT and thermogenesis [39,40]. We thus assessed whether UCP1$^+$ cell-specific inhibition of ceramide synthesis could alter energy expenditure when animals were housed at thermoneutrality such that BAT was not activated. An independent cohort of control and *Sptlc2*$^{\delta Ucp1}$ mice were maintained under thermoneutral (30 °C) conditions for 12 weeks. Under these conditions, all of the effects of *Sptlc2* ablation on energy and glucose homeostasis were lost (Suppl. Figure 3A–N). These data are consistent with our prior observations that ceramides work primarily by modulating activation of BAT and sWAT by β-adrenergic stimuli [14]. In the absence of such stimuli, the effects of ceramide depletion are negligible. In fact, we observed a slight decrease in BAT weight (Suppl. Figure 3C,A slight worsening of glucose tolerance (Suppl. Figure 3D–E), suggesting that sphingolipids may also play essential roles under thermoneutral conditions.

3.3. Inducing ceramide accumulation in UCP1$^+$-cells decreases energy expenditure

The vast majority of studies investigating the role of ceramides in obesity and metabolic disorders in rodents have relied on loss-of-ceramide interventions, much like those described in the preceding paragraphs. While these studies invariably suggest roles for

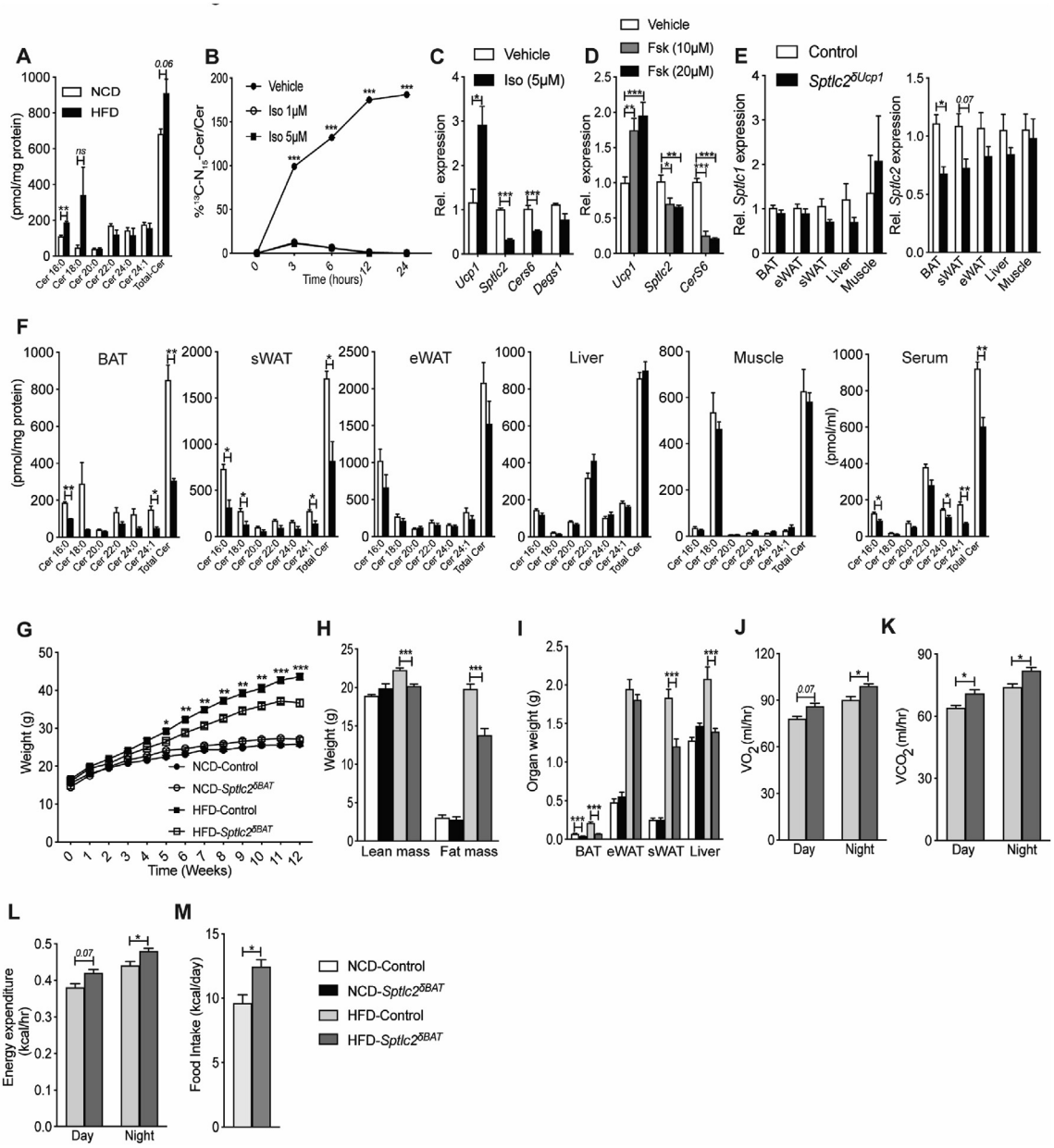

Figure 1: Mice lacking *Sptlc2* in UCP1^{+} cells are resistant to diet-induced obesity and display increased energy expenditure . (A) Ceramide content in BAT isolated from C57Bl6/J mice fed normal chow (NCD) and high-fat diets (HFD) for 12 weeks (N = 4 per group). (B) Incorporation of L-serine-$^{13}C_3$,^{15}N into ceramide in primary brown adipocytes treated with isoproterenol (Iso) (N = 4 per group). (C) mRNA expression of *Ucp1* or ceramide biosynthetic genes *Sptlc2, CerS6* and *Degs1* in primary brown adipocytes treated with isoproterenol (Iso) for 24 h (N = 4 per group). (D) mRNA expression of *Ucp1* or ceramide biosynthetic genes *Sptlc2* and *CerS6* in immortalized brown adipocytes treated with forskolin (Fsk) for 6-hrs (N = 6 per group). (E) *Sptlc1 and 2* transcript levels were assessed by qPCR. (F) Ceramide (Cer) content was assessed in various tissues by mass spectrometry (N = 5 per group). (G–M) *Sptlc2*$^{\delta Ucp1}$ mice and *Sptlc2*$^{fl/fl}$ controls were fed NCD or HFD for 12 weeks. (G) Body mass was determined weekly. (H) Fat and lean mass were quantified by NMR, and (I) organ weight was determined following euthanasia (N = 10–15 animals per group). Two weeks prior to euthanasia, animals were placed in metabolic cages (CLAMS) from Columbus Instruments. During the subsequent 3 days, (J) oxygen consumption (VO_2), (K) carbon dioxide production (VCO_2), (L) energy expenditure, and (M) food intake was quantified (N = 10–11 animals per group). Abbreviations: eWAT: epididymal fat pad, Rel.: relative; sWAT: subcutaneous fat pad. Values are expressed as mean ± SEM, *p < 0.05, **p < 0.001, and ***p < 0.0001 vs control.

ceramides in cardiometabolic disease, they have not addressed whether the increase in ceramides is sufficient to drive metabolic dysfunction in the absence of other obesogenic insults. To fully assess the consequences of ceramide accumulation in UCP1^{+}-cells, we generated mice lacking a key gene involved in ceramide degradation (i.e., the acid ceramidase gene *Asah1*), which we presumed would lead to a buildup of ceramides and other sphingolipids due to a slowing of ceramide degradation. This approach has proven efficacious in cultured cells, in which we showed that ASAH1 inhibition increases ceramides and alters insulin signaling [41]. We crossed mice carrying a loxP-flanked *Asah1* allele [31] with the aforementioned mice expressing Cre-recombinase under control of the UCP1 promoter [30]. The resulting *Asah1*$^{\delta Ucp1}$ mice had reduced *Asah1* mRNA expression (60% reduction in BAT and 20% in sWAT, but no change in other tissues) (Figure 3A). This intervention significantly increased levels of several ceramide species, as well as

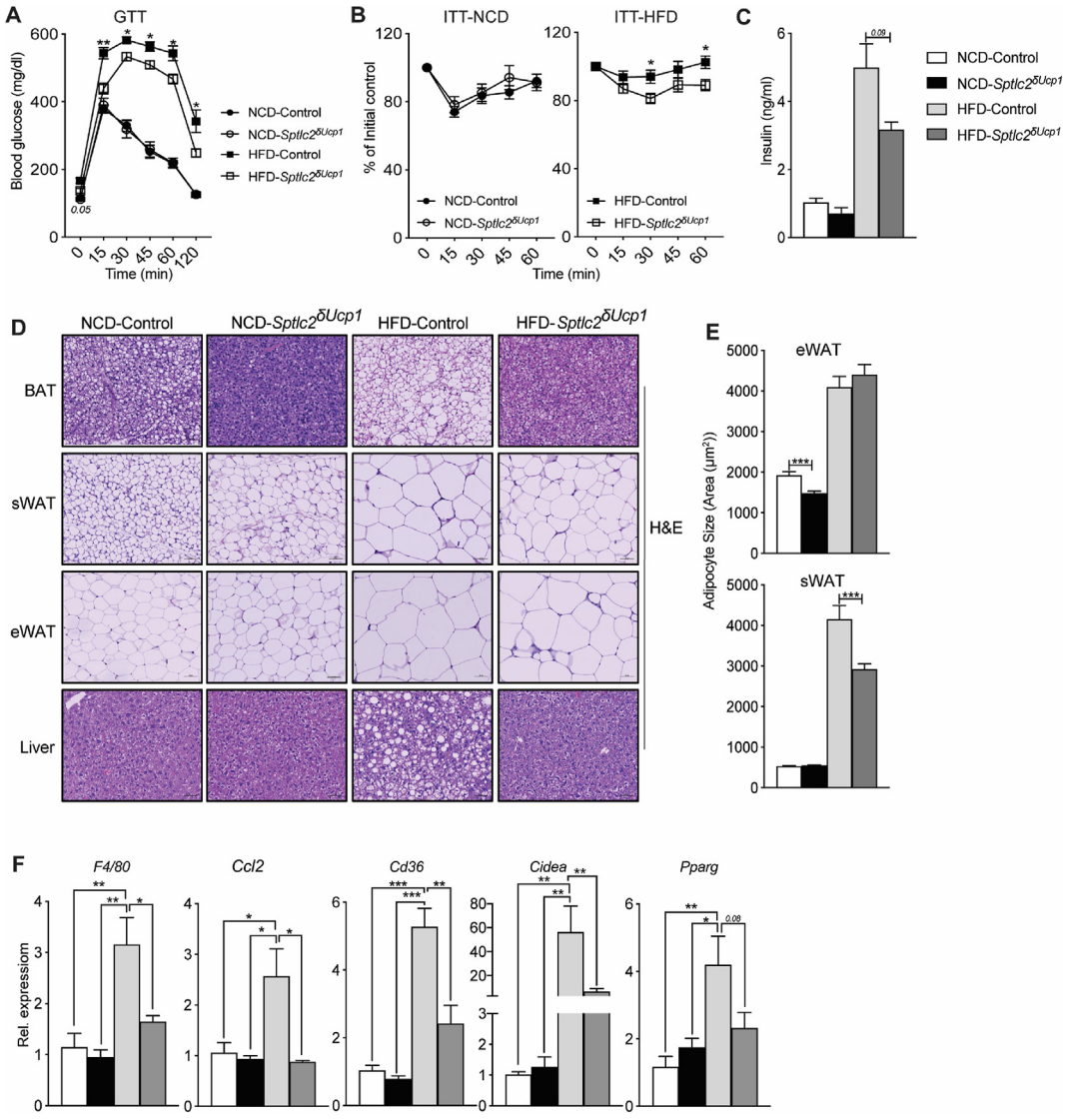

Figure 2: Mice lacking *Sptlc2* in UCP1^{+} cells are resistant to diet-induced glucose intolerance and hepatic steatosis. (A) Glucose and (B) insulin tolerance tests were performed on *Sptlc2*$^{\delta Ucp1}$ and *Sptlc2*$^{fl/fl}$ (control) mice that had been fed NCD or HFD for 10 weeks (N = 10–15 animals per group) (Legends for Figure A are the same as those in B). Following euthanasia, (C) serum insulin was quantified (N = 10 animals per group) and (D) adipose tissues and livers were evaluated histologically (H&E staining; N = 3–4 animals per group). (E) The images were evaluated to quantify adipocyte size. (F) Livers were assessed for transcripts associated with hepatic steatosis using qPCR (N = 4 animals per group). Values are expressed as mean ± SEM, *p < 0.05. *p < 0.05; **p < 0.01; ***p < 0.001.

total sphingomyelin in BAT (Figure 3B and Suppl. Fig. 4B). We also observed decreases in sWAT and eWAT sphinganine (Suppl. Fig. 4C), but not sphingosine (Suppl. Fig. 4D). Dihydroceramides were unaffected (Suppl. Fig 4A).

Although the control and *Asah1*$^{\delta Ucp1}$ mice had indistinguishable body weights at the time of weaning, *Asah1*$^{\delta Ucp1}$ mice acquired more body weight on both the NCD and HFD (Figure 3C) due to increases in fat and liver mass (Figure 3D,E). The *Asah1*$^{\delta Ucp1}$ mice had reduced oxygen consumption, CO_2 production, and energy expenditure when fed HFD (Figure 3F–H). They were not significant in the NCD cohort, though they trended in a lower direction (Suppl. Figure 4E–G). Changes in locomotor activity, RER, or food intake were either small or nonsignificant (Suppl. Figure 4H–K, Suppl. Fig.4N–R). *Asah1* depletion impaired glucose and insulin tolerance, although this was only apparent in the animals fed the HFD (Figure 3I–K and Suppl. Fig.4L–M). Histological evaluation of the adipose beds revealed that *Asah1*$^{\delta Ucp1}$ mice accumulated more lipid in BAT under NCD conditions, an effect that was exacerbated by HFD (Figure 3L). *Asah1*$^{\delta Ucp1}$ mice also exhibited an increase in adipocyte size under NCD and HFD feeding and accumulated more fat in the liver under both feeding regimens (Figure 3L–M).

These data indicate that *Asah1* depletion from UCP1^{+}-cells was sufficient to induce weight gain, decrease energy expenditure, and impair glucose and lipid metabolism, with the HFD regimen generally producing a more exaggerated phenotype.

3.4. Ceramides alter mitochondrial structure and bioenergetics

We next sought to investigate the mechanisms through which ceramides impair BAT thermogenesis and diminish organismal energy expenditure. To gauge whether changing BAT ceramides influenced heat production, we measured surface temperature above the intrascapular region of the various mouse lines using an infrared camera. In

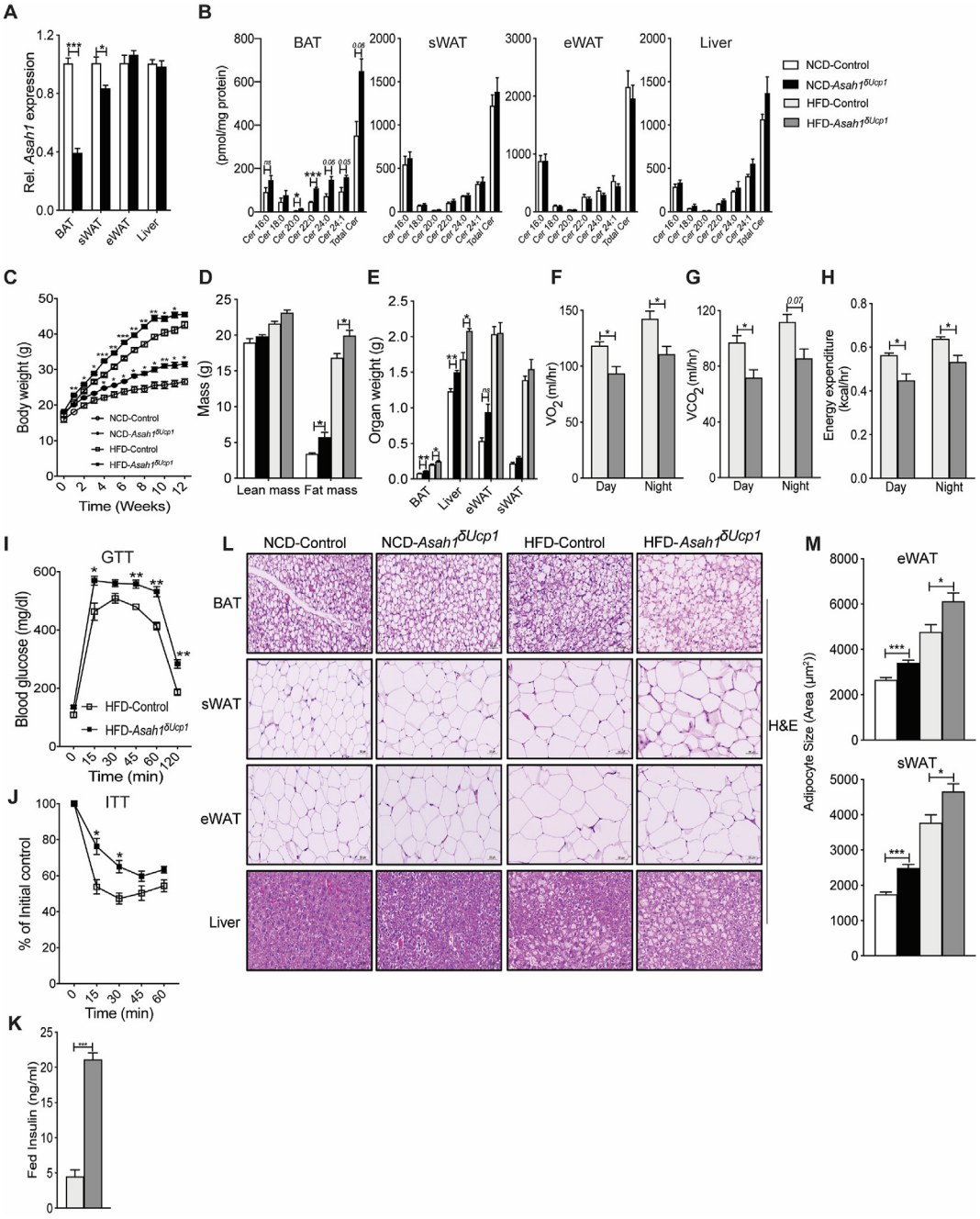

Figure 3: Mice lacking *Asah1* in UCP1$^+$ cells develop obesity and display reduced energy expenditure and impaired glucose metabolism. (A) Measurement of *Asah1* transcripts in various tissues by qPCR analysis. (B) Quantification of ceramides (Cer) by mass spectrometry (N = 3–5 animals per group). (C–J) *Asah1*$^{\delta}$Ucp1 mice and *Asah1*$^{fl/fl}$ controls were fed normal chow (NCD) or obesogenic diets (HFD) for 12 weeks. (C) Body mass was determined weekly (N = 4–11 animals per group). (D) Fat and lean mass were quantified by NMR (N = 4–7 animals per group). (E) Organ weight was determined following euthanasia (N = 4–7 animals per group). (F–H) Two weeks prior to euthanasia, animals were placed in metabolic cages (CLAMS) from Columbus Instruments. During the subsequent 3 days, (F) oxygen consumption (VO_2), (G) carbon dioxide production (VCO_2), and (H) energy expenditure were quantified (N = 5–8 animals per group). (I) Glucose and (J) insulin tolerance tests were performed when the animals had been fed on the diets for 10 weeks (N = 6–10 animals per group). (K) At the end of the studies, serum insulin was determined (N = 5–7 animals per group). (L) Adipose tissues and livers were assessed histologically (H&E staining; N = 3–4 animals per group) were evaluated. (M) The images were evaluated to quantify adipocyte size. Values are expressed as mean ± SEM, *p < 0.05. *p < 0.05; **p < 0.01; ***p < 0.001.

HFD-fed animals maintained at ambient temperature (22 °C), UCP1$^+$ cell-specific *Sptlc2* depletion increased surface temperature by 1 °C (Figure 4A–B). By contrast, UCP1$^+$cell-specific *Asah1* depletion produced the opposite result, decreasing surface temperature by 1 °C (Figure 4K–L). UCP1$^+$-driven *Sptlc2* depletion increased (Figure 4C), and UCP1$^+$-driven *Asah1* depletion decreased (Figure 4M), expression of several genes implicated in thermogenesis, including *Ucp1, Cidea, Pgc1a, Pgc1b, Cox7a, Cox8b, and Adrb3*. The interventions also reciprocally altered UCP1 protein expression (Figure 4D and N). BAT isolated from HFD-fed *Sptlc2*$^{\delta Ucp1}$ mice increased uncoupled

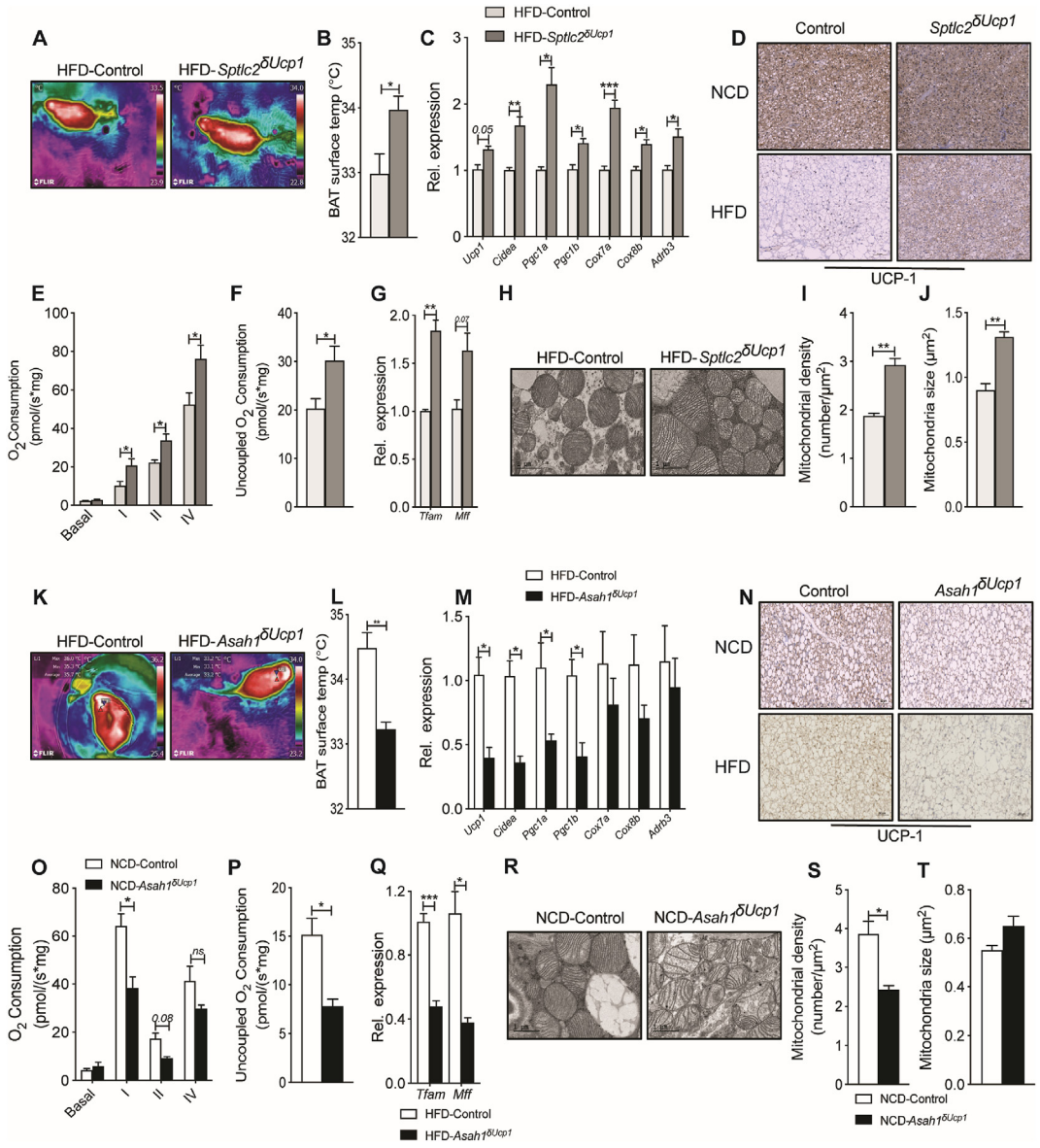

Figure 4: *Asah1* and *Sptlc2* ablation have opposing effects on BAT thermogenesis and mitochondrial structure and function. (A–B) BAT surface temperature was assessed in *Sptlc2*$^{\delta}$Ucp1 mice and *Sptlc2*$^{fl/fl}$ controls fed HFD diets for 40 weeks using an infrared camera. Temperature across the indicated region was quantified using FLIR-Tools-Software (N = 5–7 animals per group). (C) BAT genes related to mitochondrial biogenesis or thermogenesis were evaluated by qPCR (N = 5 animals per group). (D) Following euthanasia, BAT depots obtained from *Sptlc2*$^{\delta}$Ucp1 mice and *Sptlc2*$^{fl/fl}$ controls fed NCD and HFD diet for 12 weeks were evaluated by immunohistochemistry with antibodies recognizing UCP1 (N = 4 animals per group). At study termination, tissues shown in (D) were assessed for (E) mitochondrial complex activity and (F) uncoupled respiration (N = 4 animals per group), (G) qPCR measurement of mitochondrial biogenesis markers (N = 5 animals per group), and (H) transmission electron microscopy. (I) Mitochondrial density and (J) size (N = 4 animals per group) were analyzed from the transmission electron micrographs. (K–L) BAT surface temperature was assessed in *Asah1*$^{\delta}$Ucp1 mice and *Asah1*$^{fl/fl}$ controls fed a HFD (N = 6–7 animals per group). (M) Genes related to mitochondrial biogenesis or thermogenesis were evaluated by qPCR (N = 4 animals per group). (N) Following euthanasia, BAT depots obtained from *Asah1*$^{\delta}$Ucp1 mice and *Asah1*$^{fl/fl}$ controls fed NCD and HFD diets for 12 weeks were evaluated by immunohistochemistry with antibodies recognizing UCP1 (N = 4 animals per group). At study termination, tissues in (N) were assessed for (O) mitochondrial complex activity and (P) uncoupled respiration (N = 3 animals per group), (Q) qPCR measurement of mitochondrial biogenesis markers (N = 4 animals per group), and (R) transmission electron microscopy. Transmission electron micrographs. (S) Mitochondrial density and (T) size (N = 4 animals per group) were analyzed from the transmission electron micrographs (N = 3 animals per group) were analyzed in brown adipose tissue-isolated *Sptlc2*$^{\delta}$Ucp1 mice and *Sptlc2*$^{fl/fl}$ controls was determined following 12 weeks of HFD feeding. Values are expressed as mean ± SEM, *p < 0.05. *p < 0.05; **p < 0.01; ***p < 0.001.

respiration (Figure 4E–F) and enhanced activity of electron transport (ETC) chain complexes I, II, and IV. Conversely, BAT from HFD-fed *Asah1*$^{\delta Ucp1}$ mice diminished uncoupled respiration and ETC complex I, II, and IV activity (Figure 4O–P).

We also conducted an extensive analysis of mitochondrial health in the BAT depots following either *Sptlc2* or *Asah1* deletion in UCP1^{+} cells. The interventions reciprocally altered mRNA expression of key mitochondrial biogenic markers *Tfam* and *Mff* (increased in BAT of *Sptlc2*$^{\delta Ucp1}$ mice and decreased in BAT of *Asah1*$^{\delta Ucp1}$ mice) (Figure 4G and 4Q). Transmission electron microscopy revealed that BAT from HFD-fed *Sptlc2*$^{\delta Ucp1}$ mice increased mitochondrial density and size (Figure 4H–J), while BAT from HFD-fed *Asah1*$^{\delta Ucp1}$ mice had reduced

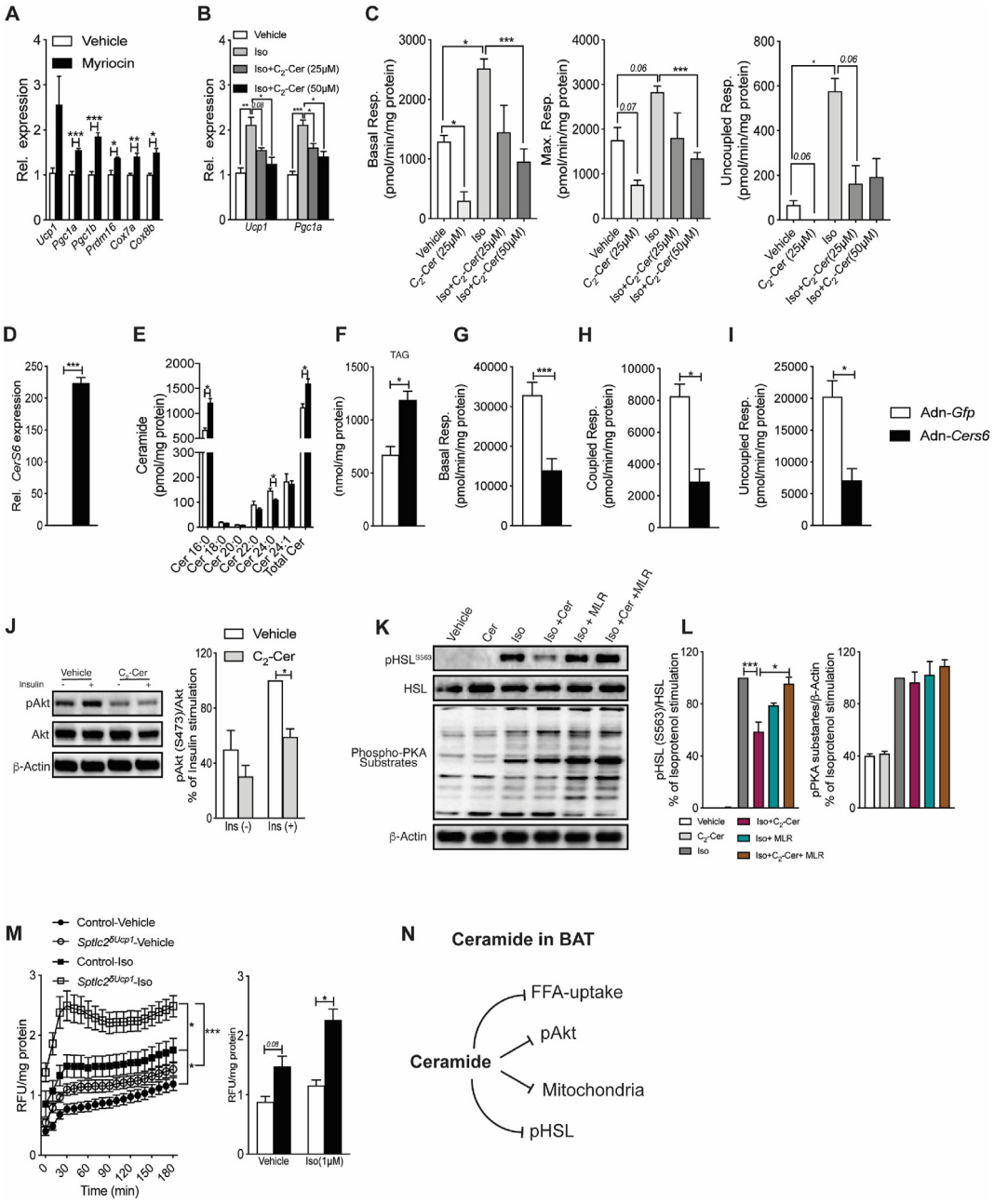

Figure 5: Ceramides have cell autonomous effects on fuel metabolism in primary brown adipocytes. Primary brown adipocytes were treated with (A) myriocin (10 μM) or (B–C) isoproterenol (1 μM) +/− C_2-ceramide as described in Materials and Methods. (A–B) Thermogenic genes were assessed by qPCR and (C) respiration was assessed by respirometry. Data are representative of 3 independent experiments completed with 4 replicates. Primary brown adipocytes were incubated with adenoviruses encoding for either green fluorescent protein (*Gfp*) or mouse-*CerS6* (D–G). Following 48 h of transfection (D) mRNA expression of *CerS6* was quantified by qPCR, (E–F) Ceramide and triglyceride content were determined by mass spectrometry and (G–I) respiration was assessed by respirometry. (J) Primary brown adipocytes were treated with vehicle or C_2-ceramide (Cer) for 2 h prior to stimulating with insulin (1 μM, 10 min). Lysates were resolved by sodium dodecyl sulfate polyacrylamide gel electrophoresis (SDS-PAGE) and western blots were performed using antibodies recognizing phosphorylated (P-Akt) or total Akt (N = 3 independent experiments). (K) Western blots and (L) quantification depicting isoproterenol (Iso) induced phosphorylation of pHSL (S563 phosphorylation sites) following treatment with C_2-ceramide (Cer, 50 μM) for 4 h followed by treatment with the PP2A inhibitor microcystin-LR (MLR) for 1 h in primary brown adipocytes (N = 3 independent experiments). (M) FFA uptake in primary brown adipocytes isolated from control and *Sptlc2*$^{\delta}$Ucp1 mouse (N = 5–7 per group). (N) Schematic summarizing the discrete mechanisms linking ceramides to changes in BAT metabolism. Values are expressed as mean ± SEM, *p < 0.05. *p < 0.05; **p < 0.01; ***p < 0.001.

mitochondrial density and a marked reduction in mitochondrial cristae density and morphology (Figure 4S–T).

We next investigated whether the effects described above could be recapitulated in brown adipocytes analyzed *in vitro.* Treating primary brown adipocytes with the SPT inhibitor myriocin increased expression of genes involved in the thermogenic program (e.g., *Ucp1*, *Pgc1a*, etc.) (Figure 5A). By contrast, adding exogenous short-chain C_2- ceramides blocked isoproterenol-driven induction of these genes (Figure 5B), as well as its stimulation of basal, maximal, and uncoupled respiration (Figure 5C). To further interrogate whether the effects could be

mediated by endogenous C_{16}-ceramide species, which were previously identified as a potentially toxic ceramide metabolite [33,35], we overexpressed *CerS6* in primary brown adipocytes *in vitro* using recombinant adenovirus. This intervention elevated expression of *CerS6* (Figure 5D) and C_{16}-ceramides (Figure 5E). Other sphingolipids, such as the sphingomyelins sphinganine and sphingosine, were unaffected (Suppl. Fig. 1J-L). The increase in C_{16}-ceramides led to increased accumulation of triglycerides (Figure 5F) and compromised mitochondrial respiration (Figure 5G—I).

3.5. Ceramides alter fuel availability

BAT uses fatty acids and glucose derived from intracellular stores and/or peripheral tissues to fuel thermogenesis [42—45]. We identified several mechanisms by which intracellular ceramides influence the availability of these substrates. (a) We previously demonstrated that lowering ceramides increases glucose uptake into BAT [14]. Ceramides likely achieve this in BAT by inhibiting Akt/PKB, a serine/threonine kinase that promotes glucose transporter translocation (Figure 5J). (b) Ceramides block lipolysis by inhibiting activation of hormone-sensitive lipase (HSL) by isoproterenol (Figure 5K—L), but not by affecting expression of lipolytic genes *Lipe* and *Atgl* (Suppl. Fig. 2P). Microcystine-LR (MLR), an inhibitor of the ceramide-target protein phosphatase 2A (PP2A), negated this ceramide effect (Figure 5K—L). (c) Lastly, ceramides may modulate isoproterenol-stimulated fatty acid import, as primary brown adipocytes isolated from *Sptlc2*$^{\delta Ucp1}$ mice displayed accelerated rates of lipid uptake (Figure 5M).

4. DISCUSSION AND CONCLUSION

Blocking synthesis of sphingolipids, such as ceramides, ameliorates insulin resistance, dyslipidemia, and hepatic steatosis and prevents progression of diabetes, atherosclerosis, and cardiovascular disease [46,47]. The data presented above suggest that a sizable fraction of these disease-causing sphingolipid effects result from actions in thermogenic adipocytes, which can exert a powerful influence on rodent metabolism. In these cells, interventions that either increase or decrease ceramides or other biosynthetic sphingolipid intermediates alter mitochondrial morphology and bioenergetics and influence glucose and lipid metabolism. In addition to showing the protective effects of sphingolipid depletion, this study is one of the first to demonstrate the consequence of selective induction of sphingolipid synthesis intermediates *in vivo*. Remarkably, inhibiting ceramide deacylation by acid ceramidase was sufficient to induce many features of the metabolic syndrome and to greatly enhance the complications of obesity.

These new findings clarify to the aforementioned controversy in the literature regarding the consequences of SPT inactivation in adipocytes. We surmise that the lipodystrophy observed by other groups following adipose-specific depletion of *Sptlc2* or *Sptlc1* [28,29] is due to impairments in adipocyte differentiation. Indeed, we have shown that SPT inhibitors block adipocyte differentiation of pre-adipocytes studied *ex vivo* [14]. Conversely, Gohlke et al. demonstrated that ceramides inhibit brown adipocyte development and differentiation [48]. Regardless, the studies described herein using UCP1-driven Cre unequivocally reveal that ceramides are bioactive nutrient signals in the mature, fully-differentiated thermogenic adipocyte.

One limitation of the manuscript relates to the challenge of determining which ceramide—or whether a precursor or ceramide metabolite—is the bioactive species that impairs BAT function. For example, depletion of *Sptlc2* and *Asah1* are likely to affect other sphingolipid species, including dihydroceramides or ceramide-1-phosphate. We measured the former, and it frequently tracks closely with ceramides. Nonetheless, the preponderance of literature indicates that ceramides, rather than dihydroceramides, are the bioactive signaling lipids. Indeed, we recently demonstrated that ablating the dihydroceramide desaturase-1, which inserts the double-bond into ceramides, increases dihydroceramide/ceramide ratios while improving adipose function and metabolic homeostasis [20]. Thus, we surmise that ceramides are more likely to serve as the bioactive molecule. We acknowledge that ceramide-1-phosphate., which is not measured by our sphingolipidomic platform, is a potential contributor to the pathogenic features of the tissue.

Several mechanistic studies support the idea that ceramides are the relevant bioactive sphingolipid that controls adipose function. In particular, we and others have identified the following cellular processes that were reciprocally regulated by either increases or decreases in ceramides in UCP1^{+}-cells (summarized in Figure 5N).

(i) Ceramides impaired mitochondrial complex activity and β-oxidation, altered mitochondrial morphology, and modulated expression of markers of mitochondrial dynamics, including *Tfam* and *Mff.* These data are consistent with prior studies showing that C_{16}-derived sphingolipids interact with MFF to promote mitochondrial fragmentation [32].
(ii) Ceramides slow lipolysis by activating the PP2A-dependent phosphorylation of HSL.
(iii) Ceramides disrupt glucose uptake by impairing Akt/PKB. We have reported previously that this results from two separable pathways that are downstream of ceramide, one involving a PKCζ-dependent phosphorylation on the enzyme's pH domain and another through the PP2A-dependent dephosphorylation of the enzyme's catalytic domain [49—51].

We speculate that these mechanisms are part of an evolutionarily-conserved pathway originally intended to protect cells by lowering levels of detergent-like fatty acids [46]. Specifically, the actions would reduce mitochondrial efficiency, decrease availability of glucose—and thus increase reliance on fatty acids—for energy production, and block the release of fatty acids from lipid droplets. The remarkable fact that these processes were changed in oppositional ways by *Sptlc2* and *Asah1* depletion *in vivo* provides the most convincing data to date that these are key ceramide-driven mechanisms accounting for ceramide-driven cardiometabolic disease.

Although these data do not identify the precise ceramide species (i.e., which acyl-chain) mediates adipose function, Brüning et al. have found that CERS6-derived C_{16}-ceramides, rather than very long-chain ceramides, are the key bioactive species that influence adipose function [32,33,52]. Our studies supported this, as we found that inhibiting production of very long-chain ceramides (e.g., C_{24} and $C_{24:1}$) led to compensatory increases in C_{16} ceramides and a worsening of metabolic control. Nonetheless, the data in this manuscript do not provide further clarity. The sphingolipid changes we observed, which were obtained under NCD conditions, revealed changes in multiple ceramide species. Based on the data in this manuscript, we cannot rule out roles for sphingolipids beyond C_{16} ceramides.

Several labs, including ours, have previously shown that ceramides induce CD36 translocation and stimulate fatty acid uptake into the liver [20,53]. We were thus intrigued to evaluate whether ceramides would alter fatty acid uptake in brown adipocytes, particularly in the presence of stimuli, such as isoproterenol, which increase fatty acid uptake. Interestingly, the *Sptlc2*$^{\delta Ucp1}$ animals displayed enhanced

isoproterenol-induced fatty acid uptake into brown adipocytes. Future studies on the regulation of fatty acid uptake by ceramides, in the presence and absence of stimuli like isoproterenol, are warranted. Collectively, these studies in the brown adipocyte reveal the importance of ceramides as metabolic regulators and provide new mechanistic details about this important class of nutrient signals. Enzymes controlling tissue ceramides are attractive therapeutic targets that hold promise for a broad range of cardiometabolic disease conditions.

AUTHOR CONTRIBUTIONS

B.C. conceived the project, designed the overall research plan, wrote the manuscript with assistance from S.A.S. B.C, L.Y, and C.L.T, performed experiments, and analyzed data. J.A.M and J.C. conducted lipid analysis. E.H.S and Y.H provided critical mouse lines used in this study. W.L.H assisted in manuscript review.

ACKNOWLEDGMENT

The authors would like to thank Donald Atkinson and Liping Wang for their excellent management of the laboratory and the outstanding personnel at the Metabolomics, Histology, Imaging, and Metabolic Phenotyping Cores at the Health Sciences Center of the University of Utah for technical advice. The authors received research support from the National Institutes of Health (DK115824, DK116888, and DK116450 to SAS; DK115824 and DK124326 to B.C; and DK108833 to WLH), the Juvenile Diabetes Research Foundation (JDRF 3-SRA-2019-768-A-B to SAS and JDRF 3-SRA-2019-768-A-B to WLH), the American Diabetes Association (to SAS), the American Heart Association (to SAS), the Margolis Foundation (to SAS), and the USDA (2019-67018-29250 to B.C.).

CONFLICT OF INTEREST

S.A.S is a consultant and shareholder with Centaurus Therapeutics. All authors have no conflict to be disclosed at this time.

APPENDIX A. SUPPLEMENTARY DATA

Supplementary data to this article can be found online at https://doi.org/10.1016/j.molmet.2020.101145.

REFERENCES

[1] Smith, R.E., 1964. Thermoregulatory and adaptive behavior of Brown adipose tissue. Science 146(3652):1686—1689.

[2] Nedergaard, J., Cannon, B., 2010. The changed metabolic world with human brown adipose tissue: therapeutic visions. Cell Metabolism 11(4):268—272.

[3] Rosen, E.D., Spiegelman, B.M., 2006. Adipocytes as regulators of energy balance and glucose homeostasis. Nature 444(7121):847—853.

[4] Tran, T.T., Kahn, C.R., 2010. Transplantation of adipose tissue and stem cells: role in metabolism and disease. Nature Reviews Endocrinology 6(4):195—213.

[5] Chouchani, E.T., Kazak, L., Spiegelman, B.M., 2019. New advances in adaptive thermogenesis: UCP1 and beyond. Cell Metabolism 29(1):27—37.

[6] Kajimura, S., Spiegelman, B.M., Seale, P., 2015. Brown and beige fat: physiological roles beyond heat generation. Cell Metabolism 22(4):546—559.

[7] Cohen, P., Spiegelman, B.M., 2015. Brown and beige fat: molecular parts of a thermogenic machine. Diabetes 64(7):2346—2351.

[8] Wang, Q., Zhang, M., Ning, G., Gu, W., Su, T., Xu, M., et al., 2011. Brown adipose tissue in humans is activated by elevated plasma catecholamines levels and is inversely related to central obesity. PloS One 6(6):e21006.

[9] Cypess, A.M., Lehman, S., Williams, G., Tal, I., Rodman, D., Goldfine, A.B., et al., 2009. Identification and importance of brown adipose tissue in adult humans. New England Journal of Medicine 360(15):1509—1517.

[10] van Marken Lichtenbelt, W.D., Vanhommerig, J.W., Smulders, N.M., Drossaerts, J.M., Kemerink, G.J., Bouvy, N.D., et al., 2009. Cold-activated brown adipose tissue in healthy men. New England Journal of Medicine 360(15):1500—1508.

[11] Moonen, M.P.B., Nascimento, E.B.M., van Marken Lichtenbelt, W.D., 2019. Human brown adipose tissue: underestimated target in metabolic disease? Biochimica et Biophysica Acta (BBA) - Molecular and Cell Biology of Lipids 1864(1):104—112.

[12] Pfannenberg, C., Werner, M.K., Ripkens, S., Stef, I., Deckert, A., Schmadl, M., et al., 2010. Impact of age on the relationships of brown adipose tissue with sex and adiposity in humans. Diabetes 59(7):1789—1793.

[13] Merrill Jr., A.H., 2002. De novo sphingolipid biosynthesis: a necessary, but dangerous, pathway. Journal of Biological Chemistry 277(29):25843—25846.

[14] Chaurasia, B., Kaddai, V.A., Lancaster, G.I., Henstridge, D.C., Sriram, S., Galam, D.L., et al., 2016. Adipocyte ceramides regulate subcutaneous adipose browning, inflammation, and metabolism. Cell Metabolism 24(6):820—834.

[15] Luukkonen, P.K., Sadevirta, S., Zhou, Y., Kayser, B., Ali, A., Ahonen, L., et al., 2018. Saturated fat is more metabolically harmful for the human liver than unsaturated fat or simple sugars. Diabetes Care 41(8):1732—1739.

[16] Luukkonen, P.K., Zhou, Y., Sadevirta, S., Leivonen, M., Arola, J., Oresic, M., et al., 2016. Hepatic ceramides dissociate steatosis and insulin resistance in patients with non-alcoholic fatty liver disease. Journal of Hepatology 64(5):1167—1175.

[17] Kolak, M., Gertow, J., Westerbacka, J., Summers, S.A., Liska, J., Franco-Cereceda, A., et al., 2012. Expression of ceramide-metabolising enzymes in subcutaneous and intra-abdominal human adipose tissue. Lipids in Health and Disease 11:115.

[18] Kolak, M., Westerbacka, J., Velagapudi, V.R., Wagsater, D., Yetukuri, L., Makkonen, J., et al., 2007. Adipose tissue inflammation and increased ceramide content characterize subjects with high liver fat content independent of obesity. Diabetes 56(8):1960—1968.

[19] Coen, P.M., Hames, K.C., Leachman, E.M., DeLany, J.P., Ritov, V.B., Menshikova, E.V., et al., 2013. Reduced skeletal muscle oxidative capacity and elevated ceramide but not diacylglycerol content in severe obesity. Obesity 21(11):2362—2371.

[20] Chaurasia, B., Tippetts, T.S., Mayoral Monibas, R., Liu, J., Li, Y., Wang, L., et al., 2019. Targeting a ceramide double bond improves insulin resistance and hepatic steatosis. Science 365(6451):386—392.

[21] Zhang, Q.J., Holland, W.L., Wilson, L., Tanner, J.M., Kearns, D., Cahoon, J.M., et al., 2012. Ceramide mediates vascular dysfunction in diet-induced obesity by PP2A-mediated dephosphorylation of the eNOS-Akt complex. Diabetes 61(7):1848—1859.

[22] Bikman, B.T., Guan, Y., Shui, G., Siddique, M.M., Holland, W.L., Kim, J.Y., et al., 2012. Fenretinide prevents lipid-induced insulin resistance by blocking ceramide biosynthesis. Journal of Biological Chemistry 287(21):17426—17437.

[23] Holland, W.L., Brozinick, J.T., Wang, L.P., Hawkins, E.D., Sargent, K.M., Liu, Y., et al., 2007. Inhibition of ceramide synthesis ameliorates glucocorticoid-, saturated-fat-, and obesity-induced insulin resistance. Cell Metabolism 5(3):167—179.

[24] Hojjati, M.R., Li, Z., Zhou, H., Tang, S., Huan, C., Ooi, E., et al., 2005. Effect of myriocin on plasma sphingolipid metabolism and atherosclerosis in apoE-deficient mice. Journal of Biological Chemistry 280(11):10284—10289.

[25] Park, T.S., Rosebury, W., Kindt, E.K., Kowala, M.C., Panek, R.L., 2008. Serine palmitoyltransferase inhibitor myriocin induces the regression of atherosclerotic plaques in hyperlipidemic ApoE-deficient mice. Pharmacological Research 58(1):45—51.

[26] Park, T.S., Panek, R.L., Mueller, S.B., Hanselman, J.C., Rosebury, W.S., Robertson, A.W., et al., 2004. Inhibition of sphingomyelin synthesis reduces atherogenesis in apolipoprotein E-knockout mice. Circulation 110(22):3465—3471.

[27] Ussher, J.R., Koves, T.R., Cadete, V.J., Zhang, L., Jaswal, J.S., Swyrd, S.J., et al., 2010. Inhibition of de novo ceramide synthesis reverses diet-induced insulin resistance and enhances whole-body oxygen consumption. Diabetes 59(10):2453—2464.

[28] Alexaki, A., Clarke, B.A., Gavrilova, O., Ma, Y., Zhu, H., Ma, X., et al., 2017. De novo sphingolipid biosynthesis is required for adipocyte survival and metabolic homeostasis. Journal of Biological Chemistry 292(9):3929—3939.

[29] Lee, S.Y., Lee, H.Y., Song, J.H., Kim, G.T., Jeon, S., Song, Y.J., et al., 2017. Adipocyte-specific deficiency of de novo sphingolipid biosynthesis leads to lipodystrophy and insulin resistance. Diabetes 66(10):2596—2609.

[30] Kong, X., Banks, A., Liu, T., Kazak, L., Rao, R.R., Cohen, P., et al., 2014. IRF4 is a key thermogenic transcriptional partner of PGC-1alpha. Cell 158(1):69—83.

[31] Eliyahu, E., Shtraizent, N., Shalgi, R., Schuchman, E.H., 2012. Construction of conditional acid ceramidase knockout mice and in vivo effects on oocyte development and fertility. Cellular Physiology and Biochemistry 30(3):735—748.

[32] Hammerschmidt, P., Ostkotte, D., Nolte, H., Gerl, M.J., Jais, A., Brunner, H.L., et al., 2019. CerS6-Derived sphingolipids interact with Mff and promote mitochondrial fragmentation in obesity. Cell 177(6):1536—1552 e1523.

[33] Turpin, S.M., Nicholls, H.T., Willmes, D.M., Mourier, A., Brodesser, S., Wunderlich, C.M., et al., 2014. Obesity-induced CerS6-dependent C16:0 ceramide production promotes weight gain and glucose intolerance. Cell Metabolism 20(4):678—686.

[34] Turpin-Nolan, S.M., Hammerschmidt, P., Chen, W., Jais, A., Timper, K., Awazawa, M., et al., 2019. CerS1-Derived C18:0 ceramide in skeletal muscle promotes obesity-induced insulin resistance. Cell Reports 26(1):1—10 e17.

[35] Raichur, S., Wang, S.T., Chan, P.W., Li, Y., Ching, J., Chaurasia, B., et al., 2014. CerS2 haploinsufficiency inhibits beta-oxidation and confers susceptibility to diet-induced steatohepatitis and insulin resistance. Cell Metabolism 20(5):919.

[36] Hla, T., Kolesnick, R., 2014. C16:0-ceramide signals insulin resistance. Cell Metabolism 20(5):703—705.

[37] Schweizer, S., Liebisch, G., Oeckl, J., Hoering, M., Seeliger, C., Schiebel, C., et al., 2019. The lipidome of primary murine white, brite, and brown adipocytes-Impact of beta-adrenergic stimulation. PLoS Biology 17(8): e3000412.

[38] Park, M., Kaddai, V., Ching, J., Fridianto, K.T., Sieli, R.J., Sugii, S., et al., 2016. A role for ceramides, but not sphingomyelins, as antagonists of insulin signaling and mitochondrial metabolism in C2C12 myotubes. Journal of Biological Chemistry 291(46):23978—23988.

[39] Cannon, B., Nedergaard, J., 2004. Brown adipose tissue: function and physiological significance. Physiological Reviews 84(1):277—359.

[40] Chaffee, R.R., Roberts, J.C., 1971. Temperature acclimation in birds and mammals. Annual Review of Physiology 33:155—202.

[41] Chavez, J.A., Holland, W.L., Bar, J., Sandhoff, K., Summers, S.A., 2005. Acid ceramidase overexpression prevents the inhibitory effects of saturated fatty acids on insulin signaling. Journal of Biological Chemistry 280(20):20148—20153.

[42] Chondronikola, M., Volpi, E., Borsheim, E., Porter, C., Saraf, M.K., Annamalai, P., et al., 2016. Brown adipose tissue activation is linked to distinct systemic effects on lipid metabolism in humans. Cell Metabolism 23(6):1200—1206.

[43] Iwen, K.A., Backhaus, J., Cassens, M., Waltl, M., Hedesan, O.C., Merkel, M., et al., 2017. Cold-induced Brown adipose tissue activity alters plasma fatty acids and improves glucose metabolism in men. Journal of Clinical Endocrinology & Metabolism 102(11):4226—4234.

[44] Orava, J., Nuutila, P., Lidell, M.E., Oikonen, V., Noponen, T., Viljanen, T., et al., 2011. Different metabolic responses of human brown adipose tissue to activation by cold and insulin. Cell Metabolism 14(2):272—279.

[45] Ouellet, V., Labbe, S.M., Blondin, D.P., Phoenix, S., Guerin, B., Haman, F., et al., 2012. Brown adipose tissue oxidative metabolism contributes to energy expenditure during acute cold exposure in humans. Journal of Clinical Investigation 122(2):545—552.

[46] Summers, S.A., Chaurasia, B., Holland, W.L., 2019. Metabolic messengers: ceramides. Nature Metabolism 1:1051—1058.

[47] Chaurasia, B., Summers, S.A., 2015. Ceramides - lipotoxic inducers of metabolic disorders. Trends in Endocrinology and Metabolism 26(10):538—550.

[48] Gohlke, S., Zagoriy, V., Cuadros Inostroza, A., Meret, M., Mancini, C., Japtok, L., et al., 2019. Identification of functional lipid metabolism biomarkers of brown adipose tissue aging. Mol Metab 24:1—17.

[49] Stratford, S., Hoehn, K.L., Liu, F., Summers, S.A., 2004. Regulation of insulin action by ceramide: dual mechanisms linking ceramide accumulation to the inhibition of Akt/protein kinase B. Journal of Biological Chemistry 279(35): 36608—36615.

[50] Powell, D.J., Hajduch, E., Kular, G., Hundal, H.S., 2003. Ceramide disables 3-phosphoinositide binding to the pleckstrin homology domain of protein kinase B (PKB)/Akt by a PKCzeta-dependent mechanism. Molecular and Cellular Biology 23(21):7794—7808.

[51] Blouin, C.M., Prado, C., Takane, K.K., Lasnier, F., Garcia-Ocana, A., Ferre, P., et al., 2010. Plasma membrane subdomain compartmentalization contributes to distinct mechanisms of ceramide action on insulin signaling. Diabetes 59(3): 600—610.

[52] Turpin-Nolan, S.M., Bruning, J.C., 2020. The role of ceramides in metabolic disorders: when size and localization matters. Nature Reviews Endocrinology 16(4):224—233.

[53] Xia, J.Y., Holland, W.L., Kusminski, C.M., Sun, K., Sharma, A.X., Pearson, M.J., et al., 2015. Targeted induction of ceramide degradation leads to improved systemic metabolism and reduced hepatic steatosis. Cell Metabolism 22(2):266—278.

